Fachtagung "Lasermethoden in der Strömungsmesstechnik"
9. – 11. September 2014, Karlsruhe

Wirbel im Herzen – Anwendung von Techniken zur Strömungscharakterisierung

Heart Flow Vortices – An Application of Flow Characterization Techniques

A. Slotosch, J. Schlanderer, F. Kaiser, J. Kriegseis
Karlsruhe Institute of Technology (KIT), Institute of Fluid Mechanics (ISTM)
Kaiserstr. 10, 76131 Karlsruhe, Germany

Schlagworte: Herzströmung, Wirbelidentifikation, Finite-Time Lyapunov Exponent (FTLE)
Key words: heart flow, vortex detection, Finite-Time Lyapunov Exponent (FTLE)

Abstract

The present work addresses the identification and characterization of vortical flow structures as occurring during the pumping cycle of human hearts. The inflow phase of this cycle is largely dominated by the formation of a vortex ring when blood enters the left ventricle (LV) through the mitral valve. In case of healthy hearts, this vortex ensures both, high mixing level and short residence time in the LV. As such, detailed knowledge of vortex formation and location as well as persistence of adverse recirculation zones is of prime importance to evaluate the health state of a patient's heart and predict the resulting flow manipulations of potentially necessary heart surgeries. The purpose of the present study, therefore, concentrates on a comparison of two different vortex detection methods - namely the Q-criterion and the Finite-Time Lyapunov Exponent (FTLE). Even though the former reveals an appropriate estimate on the vortex location, thus formation process and trajectory, a clear separation of a vortical structure from the surrounding flow is extremely difficult and appears somewhat arbitrary. This issue is met by application of the FTLE, which is calculated based on the Lagrangian properties of particles and consequently ensures an identification of unsteady Lagrangian coherent structures (LCS), i.e. vortices and persistent recirculation zones. Both applied methods are first applied to a generic two dimensional (2D) test case of counter-rotating vortices, so as to introduce and compare the approaches. Subsequently, three dimensional (3D) numerical data of flow through the LV is characterized by means of both approaches, which in combination provide the desired information on heart flow vortices.

Background and Objectives

Today, the overall flow topology in a healthy human heart is well known to be dominated by the formation of a vortex ring during the inflow phase (diastole), which is supposed to be responsible for the washout of the LV. Acting like a pump, the LV is responsible for the transport of fresh oxygenated blood from the lungs into the body using two valves to regulate the flow direction. After the breakup of the vortex ring into smaller structures, the flow is redirected towards the aorta (systole) forming a helical shape (Spiegel 2009). As such, the flow structure is highly unsteady and 3D. Modern imaging methods like the time-resolved 2D Doppler echocardiography allow in-situ heart-flow measurements, which in turn uncover changes of the intra-ventricular flow dynamics of diseased hearts. It is up to the examiner to determine the severity level of a heart disease like the dilative cardiomyopathy, where the residence time of blood is of particular interest; see Hendabadi *et al.* (2013). Since recircula-

tion zones may result in thrombus formation, it is beneficial to identify such regions and in turn predict flow modifications of upcoming surgical procedures.

Numerical simulations have become a valuable means to reconstruct patient specific heart flow, as the entire flow field can be determined at once. Moreover, flow field changes can be predicted as function of (simulated) heart shape modifications through surgeries. Despite the variety of post processing techniques to extract clinical relevant information, the full characterization of the flow field remains challenging. Provided that the simulation techniques appropriately mimic patient specific flow conditions, then the commonly applied local vortex detection methods (Q, Δ, λ_2) reveal the majority of overall flow features with reasonable accuracy. In contrast, no information on fluid residence times or mixing levels can be determined with local approaches. Consequently, if such information is desired, additional particle tracking algorithms or scalar transport models become necessary (Spiegel 2009). For instance, Hendabadi *et al.* (2013) successfully applied the FTLE on 2D Doppler echocardiography data of a LV and extracted flow regions of blood inserted during different heartbeats. This study demonstrated that a calculation of particle residence times from Eulerian data is possible. Despite these first promising results, the accuracy level of 2D information remains uncertain, as the 3D character of the flow is ignored during track estimation.

Applied to a 3D simulation of a healthy patient specific LV, the main objective of the present work is the comparison of local Eulerian and time-integrating Lagrangian methods, so as to identify and combine the strengths of either approach. To reduce the flow complexity and focus on the purpose of work, the heart valves are modelled as 2D porosity planes, the shape of the heart wall is averaged over five full heart beat cycles T (preset: 60 bpm / 1Hz) and blood is treated as Newtonian fluid. The flow fields are compared during the diastole of the fifth heartbeat, i.e. $4 \leq t^* = t/T \leq 4.5$, to ensure periodicity of the flow. Figure 1a) shows the corresponding stream lines that already provide some confidence on the location of the vortex ring. Two planes were defined to compare the considered detection methods: a plane along the short axis (SA) that cuts through the base and a plane along the long axis (LA) of the LV that cuts through the valve planes (compare Figure 1b)).

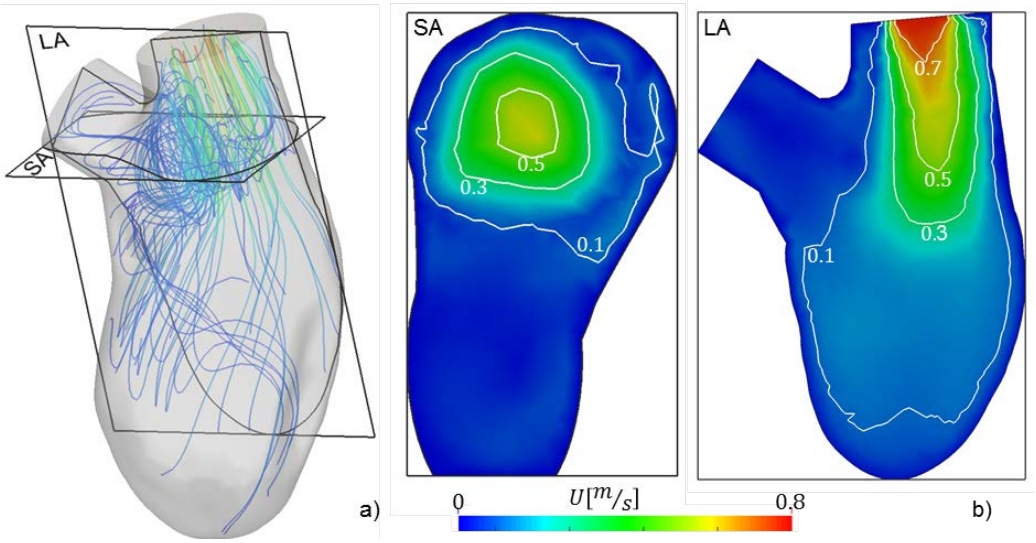

Fig. 1: LV flow at $t^* = 4.24$ visualized with a) 3D streamlines and b) contour plots colored by magnitude of velocity on 2D slices through the short axis (SA) and the long axis (LA).

The afore-mentioned artificial (yet insightful) 2D test case comprises two horizontally meandering and counter-rotating vortices, as already used by Shadden *et al.* (2005). This periodically varying double-gyre is expressed by the analytical stream-function

$$\psi(x, y, t) = 0.1 \sin\big(\pi f(x, t)\big) \sin(\pi y), \tag{1}$$

which is evaluated over the domain $[0,2] \times [0,1]$ with

$$f(x, t) = 0.25 \sin(0.2\pi t)\, x^2 + (1 - 0.5\ \sin(0.2\pi t))\, x. \tag{2}$$

For more details on double-gyre flow please refer to Shadden *et al.* (2005) or Haller (2011).

Methods

Local vortex detection method – Q-criterion

The three most common local vortex detection methods are Q-, λ_2- and Δ-criterion, which are all evaluated from the velocity gradient tensor $\nabla\vec{u}$. Thus, the calculations for these methods can be performed point-wise and all criteria are then visualized by iso-surfaces of the resultant scalar values.

The Q-criterion introduced by Hunt *et al.* (1988) considers the difference between vorticity and strain rate. Mathematically, the quantity Q is the second invariant of the characteristic equation of $\nabla\vec{u}$ as defined by

$$Q = \frac{1}{2}\left(\left(\|\Omega_{ij}\|\right)^2 - \left(\|\epsilon_{ij}\|\right)^2\right) > 0, \tag{3}$$

where Ω_{ij} and ϵ_{ij} represent the rotation tensor and the strain rate tensor respectively. A vortex is present where $Q > 0$, i.e. where rotation predominates shear.

Note that initially both, the Δ -criterion as proposed by Chong et al. (1990) and the λ_2-criterion, as proposed by Jeong and Hussain (1995), were implemented and tested on various cases, including the flow scenarios of the double-gyre flow and the LV presented in this work. However, the results of all three local methods (Q, Δ, λ_2) did not differ all too much. Therefore, the present work only considers the Q-criterion and the focus of the study rather concentrates on the comparison with the FTLE approach. Nonetheless, it is worth to note that the main drawback of all local methods is the lack of a clear definition of a vortex boundary, because arbitrarily chosen iso-values of Q-, λ_2- or Δ indicate vortical structures and the corresponding spatial dimensions.

Finite-Time Lyapunov Exponent

LCS are material manifolds, which act as precise vortex boundaries (Grigoriev 2012). These are represented as material lines in 2D and material surfaces in 3D flows. Haller (2011) defines hyperbolic LCS as locally strongest repelling or attracting material surfaces. The LCS can be extracted by application of the FTLE. First proposed by Pierrehumbert (1991), the FTLE defined the changing distance of two initially neighboring particles over a particular integration time. An increasing distance between the particles, increases likewise the FTLE-value. Later, Haller *et al.* (2000, 2002) and Shadden *et al.* (2005) provided a profound mathematical description and a new approach to calculate fields, that nowadays are often called classical or flow-map FTLE-fields. Thereby, Shadden *et al.* defined LCS as ridges of the FTLE-field, which precisely define vortex boundaries, but also indicate flow separatrices.

Particles can be tracked forward or backward in time to reveal repelling or attracting manifolds, respectively. As the procedure is the same, only the approach to extract repelling structures (by tracking forward in time) is presented here in detail. The basic idea is to observe two particles starting at time t_0 at the position $\vec{x}_0$ and its immediate vicinity $\vec{x}_0 + \delta\vec{x}_0$. The Lyapunov exponent σ_L describes the rate of separation of the trajectories of the two particles with time and thereby gives information about the instability of the starting point according to

$$\sigma_L = \lim_{t-t_0\to 0}\lim_{\delta\vec{x}_0\to 0}\frac{1}{t-t_0}\ln\frac{\delta\vec{x}(t)}{\delta\vec{x}_0}. \tag{4}$$

In practice, the unsteady flow information is only known for finite times. Therefore, an effective finite–time exponent (see Kantz, 1994) for the FTLE is defined as

$$\sigma_{t_0}^{t} = \lim_{\delta\vec{x}_0\to 0}\frac{1}{t-t_0}\ln\frac{\delta\vec{x}(t)}{\delta\vec{x}_0}, \text{ with } t > t_0. \tag{5}$$

The separation at time t can be expressed as

$$\left\|\delta\vec{x}(t)\right\| = \exp(\sigma_{t_0}^{t}(t-t_0))\left\|\delta\vec{x}_0\right\|, \tag{6}$$

where the distance $\delta\vec{x}(t)$ between the two observed particles at time t can be described by

$$\delta\vec{x}(t) = \Phi_{t_0}^{t}(\vec{x}_0 + \delta\vec{x}_0) - \Phi_{t_0}^{t}(\vec{x}_0). \tag{7}$$

Here, the flow-map $\Phi_{t_0}^{t}$ can be calculated by seeding a particle at $\vec{x}_0$ and track it for the time t using the relation

$$\vec{x}_0 \mapsto \Phi_{t_0}^{t}(\vec{x}_0) = \vec{x}(t;\vec{x}_0,t_0), \tag{8}$$

which describes the current position of a particle that started at $(t_0, \vec{x}_0)$. Shadden *et al.* (2005) linearized Equation (7) by a Taylor series up to the first derivative,

$$\delta\vec{x}(t) = \Phi_{t_0}^{t}(\vec{x}_0 + \delta\vec{x}_0) - \Phi_{t_0}^{t}(\vec{x}_0) = \frac{\mathrm{d}\Phi_{t_0}^{t}}{\mathrm{d}\vec{x}_0}\delta\vec{x}_0 + O(\left\|\delta\vec{x}_0\right\|^2), \tag{9}$$

which introduces a second order error, but ensures a much more efficient calculation. As the gradient of the flow map $\mathrm{d}\Phi_{t_0}^{t}/\mathrm{d}\vec{x}_0 = \nabla\Phi_{t_0}^{t}$ is a real matrix, the Euclidean norm of $\delta\vec{x}(t)$ can be simplified to

$$\left\|\delta\vec{x}(t)\right\| = \sqrt{(\nabla\Phi_{t_0}^{t}\delta\vec{x}_0)^{\mathrm{T}}\nabla\Phi_{t_0}^{t}\delta\vec{x}_0} = \sqrt{(\delta\vec{x}_0)^{\mathrm{T}}(\nabla\Phi_{t_0}^{t})^{\mathrm{T}}\nabla\Phi_{t_0}^{t}\delta\vec{x}_0}. \tag{10}$$

The positive definite matrix

$$C = (\nabla\Phi_{t_0}^{t})^{\mathrm{T}}\nabla\Phi_{t_0}^{t}, \tag{11}$$

which represents the right Cauchy-Green deformation tensor, is responsible for the stretching of the infinitesimal small perpetuation with arbitrary direction $\delta\vec{x}_0$. If the direction of $\delta\vec{x}_0$ is the same as the direction of the eigenvector of C connected to the largest eigenvalue $\lambda_{\max}(C)$, the perpetuation is maximized and can be expressed as

$$\max\left\|\delta\vec{x}(t)\right\| = \sqrt{\lambda_{\max}(C)}\left\|\delta\vec{x}_0\right\|. \tag{12}$$

Inserting this information into Equation (10) leads to

$$\left\|\delta\vec{x}(t)\right\| = \exp(\sigma_{t_0}^{t}(t-t_0))\left\|\delta\vec{x}_0\right\| = \sqrt{\lambda_{\max}(C)}\left\|\delta\vec{x}_0\right\|, \tag{13}$$

where

$$\sigma_{t_0}^{t} = \frac{1}{t-t_0}\ln\sqrt{\lambda_{\max}(C)} \tag{14}$$

is called the largest FTLE for forward integration describing how strong the flow is repelled in forward time. Therefore, the ridges of the FTLE-field act as hyperbolic LCS. Applying the absolute value of the integration time $|t-t_0|$ in the above formulas the equations become applicable to both, forward integration and backward integration (to extract attracting LCS).

The FTLE-field is calculated numerically on an Eulerian grid. Hence, the result might be affected by the chosen spatial resolution. For instance, if a coarse mesh is chosen for the tracked particles, some smaller FTLE-structures may remain hidden. An even more critical parameter in the described concept is the integration time. Usually, a longer integration time leads to steeper ridges of the FTLE-field. However, in unsteady flows a material line might lose its hyperbolic character after a certain time and structures will vanish if the integration time is too long.

Results and Discussion

To emphasize the main differences between Q-criterion and FTLE, either approach will first be elaborated based on the 2D double-gyre data. Subsequently, the application on the 3D heart flow data is discussed.

double-gyre flow

The usage of an Eulerian description of the flow, i.e. the Q-criterion, enables a fast and easily computed on-site characterization. Two instantaneous snap shots (at time t_1 and t_2) are shown in Figure 2, which indicate a fifth of the perturbation period; see Eqs. (1) and (2). The upper row of Figure 2 shows the velocity vectors superimposed onto contours of Q. As seen, it is perfectly able to capture the presence of two vortices within the domain at every time point, indicated by the solid iso-lines which mark positive values of Q. Regions where no vortex is identified are found in the four corners of the domain and the vortex-vortex interface (dashed iso-lines). Observing the Q-criterion with time, the positive regions expand and contract as expected for the investigated flow field.

Obviously both, the rotatory behavior of the flow and vortex motion, are well captured by the local vortex detection method. However, at no point in time a chaotic behavior of the flow is indicated. Furthermore, it is impossible to predict the trajectory of particular fluid elements, which is essential for residence-time estimates, for instance. These shortcomings will be met by the FTLE approach in the following.

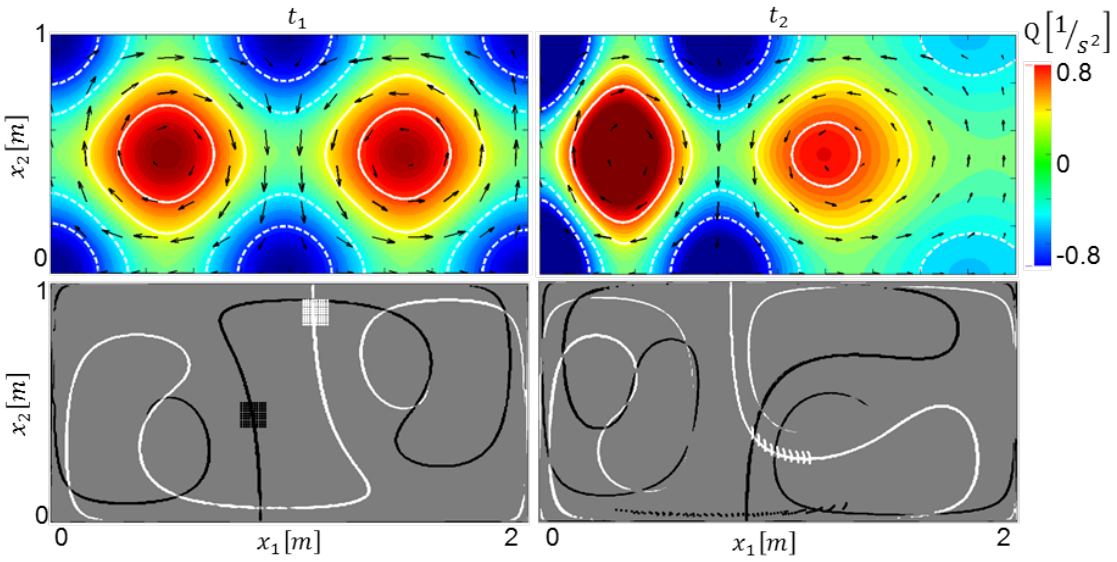

Fig. 2: analysis of the double-gyre flow field at two snap shots illustrated by (top) the application of the Q-criterion (solid lines indicate $Q > 0$, dashed lines indicate $Q < 0$) and (bottom) the FTLE method (white lines mark ridges of backward FTLE, black lines mark ridges of forward FTLE

For the FTLE-calculation, an integration time of 1.5 perturbation periods is chosen. The lower part of Figure 2 shows the evolution of LCS at identical times as used before. While the black ridges are the local maxima of the forward FTLE calculation and therefore repelling LCS, the white ridges represent attracting particle lines obtained by backward FTLE. To visualize and explain the effect of LCS, particle groups are seeded at two locations around the different manifolds. Thereby, several features of the LCS are emphasized. First, the attraction and repulsion of particles normal to the LCS can be observed. Second, a corresponding folding or stretching parallel to the LCS can be studied, which is caused by the incompressibility of the fluid. Furthermore, the separating character of LCS as material lines of negligible amounts of cross flux is demonstrated (see Shadden *et al.*, 2005).

The black ridges in Figure 2 imply a significant growth of the distance between two particles seeded near the ridge during the integration time. Note that the change of their distance to each other is not monotonic in time. The FTLE-field only provides information about the change between the start and the end of the integration time and not about its evolution. For this example the lower half of the middle axis between the two gyres acts as the main repelling feature in the flow, it can be stated, that all of the particles placed at the black ridge will reach this point during the integration time. As the white, attracting ridges act backward in time, there is no direct information about future movement of the flow in their structures. This explains why attracting and repelling particles can be parallel in one picture if the integration time is chosen very long (as done in the present example). Nevertheless, as the stable manifolds attracted particles in the past, they are as well organizing structures of the flow. However, for shorter integration times attracting and repelling structures might no longer be parallel and the influence of the different time spans becomes less and less important. Furthermore, the FTLE calculation reveals different features of the flow, depending on the chosen integration time. For long integration times it is possible to interpret the evolution of a flow beyond the boundaries of the considered flow domain, while the information about the de facto hyperbolic structures at the very moment where the integration starts could be lost. Therefore, shorter integration times are chosen regarding the heart flow to detect precise vortex boundaries.

LV flow

The transport of blood by means of vortex-ring formation is supposed to be more efficient as compared to a steady, straight jet of blood (Gharib *et al.* 2006). Therefore, a proper detection is essential for the characterization of the heart's condition and efficiency. On the left of Figure 3, the main characteristics of the inflow phase are demonstrated based on iso-surfaces of Q at two instances during the diastole. At the initial phase of the filling process ($t^* = 4.24$) of the LV the developed vortex ring is clearly visible. The SA view shows the outer diameter of the vortex ring while the LA view depicts the inner radius. Afterwards, the vortex ring is propagating through the LV and slightly tilts counter clockwise. At $t^* = 4.4$, the ring shape of the vortex ring can no longer be clearly identified as it is already significantly deformed and its breakup starts. After the tilting of the vortex, it rapidly becomes unstable and breaks down into smaller structures. Even though not shown here, it is worth to note that during the outflow phase, the Q-criterion again identifies a tubular connected structure where the blood flow forms helical streamlines.

As a vortex is connected to a pressure minimum, the identification of the vortex ring also identifies the location of a pressure minimum and its movement through the flow region. Furthermore, regions of negative Q indicate that the strain rate predominates rotation; see Equation (3). As the strain rate in a Newtonian fluid is proportional to the shear stress, minimal Q values imply maximum shear. This in fact is important information, since high rates of shear can destroy blood cells and enhance thrombus formation. This insight remains hidden, when applying the FTLE.

As already mentioned the heart flow data is evaluated with short integration times. Thereby, the inflow of the blood into the left ventricle is visualized using the backward FTLE which shows a clear vortex boundary. The right column of Figure 3 shows bell-like attracting structures in the LV during the early phase of the inflow. The blood particles entering from the left atrium impinge on the relatively slow moving blood particles in the LV, thereby get distracted and change their movement direction. They get folded normal to the detected material surface and stretched parallel to it, which indicates that an attracting manifold is revealed by the FTLE. Observing the extracted ridges from $t^* = 4.24$ to $t^* = 4.4$, a transport of the detected LCS during the diastole is clearly visible.

Blazevski and Haller (2014) state that the ridges of the FTLE-field can be interpreted as transport barriers. These findings show that the incoming blood does not mix with the present blood during the inflow phase. Such information is not accessible using a local vortex detection method. The manifold can be observed until it collides with the wall of the heart. Mixing takes place and the choice of a higher spatial grid resolution appears to be required in

order to reveal the smaller structures during the mixing process. Nonetheless, observation of those structures will be beneficial in order to extract information about the degree of mixing and the residence time of fluid elements in the LV.

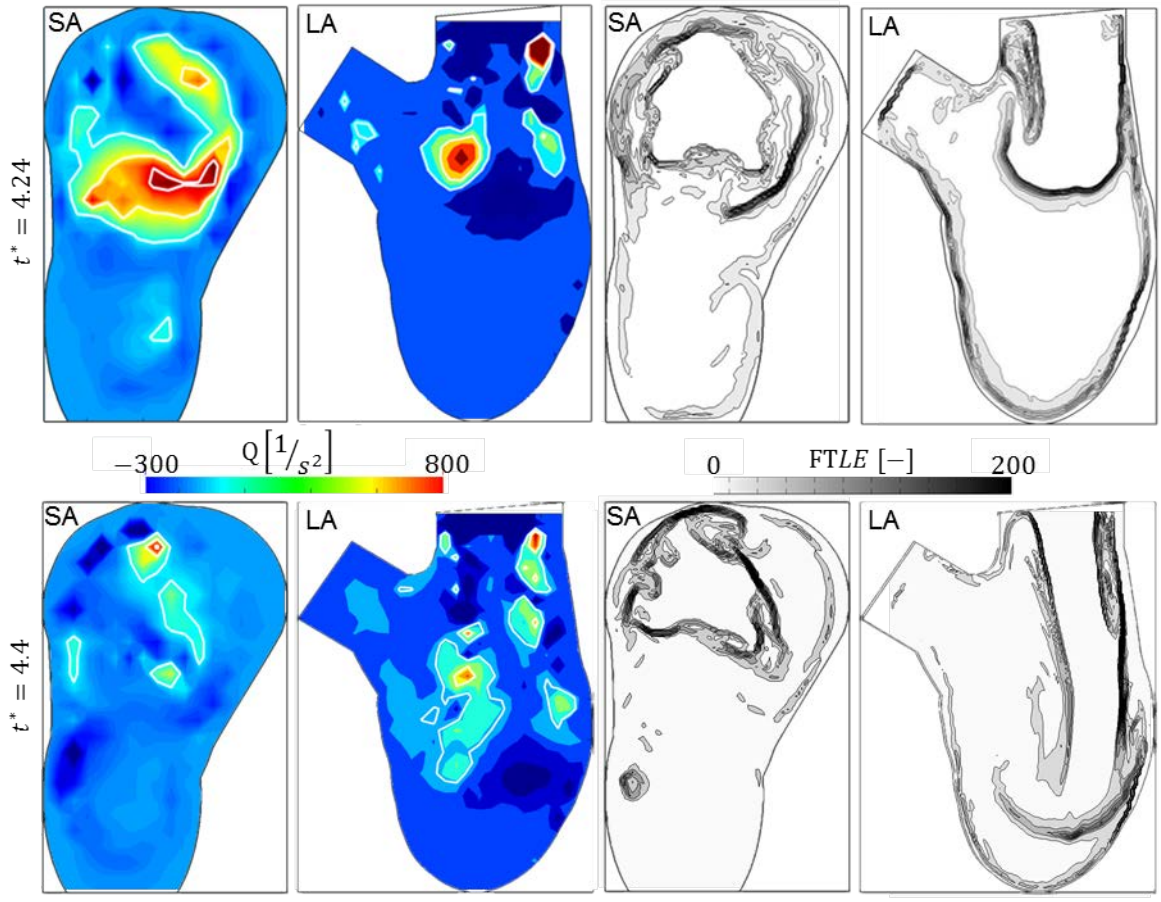

Fig. 3: Contours of (left) *Q*-criterion and (right) FTLE of LV flow displayed on SA and LA

Several difficulties are still present during the generation of the FTLE field that have to be addressed in order to judge on the quality of the presented results concerning the LV flow. For instance, the particle tracking uses a 4th order Runga-Kutta algorithm, which sometimes allows particles to leave the virtual heart model through the moving walls. As such, overestimated attracting LCS along the heart wall might be determined. Fortunately, this overprediction does not affect the inner flow region. Additionally, it turned out to be extremely challenging to extrapolate the velocity field properly outside of the heart, since a more realistic calculation of backward FTLE during the early diastole and forward FTLE during the late systole is required. To overcome this issue in the first instance, the examined time points, position of seeded particles and integration times were chosen accordingly.

Conclusions and Future Work

Both examined methods, the Q-criterion as an example for a local Eulerian vortex detection approach and the FTLE as a Lagrangian approach, are able to provide meaningful insight into LV flow properties. The Eulerian approach detects the expected vortices and therefore provides easy detection of pressure minima or flow abnormalities. Furthermore, it detects regions of high shear stress that can damage the blood cells. However, due to the continuous distribution of Q it is not possible to define clear vortex boundaries or gain information about the temporal evolution.

The skeletal structure given by the FTLE calculation of attracting and repelling manifolds provides meaningful insights about the properties of the flow during the integration time

including cause-effect relations, recirculation zones and material borders. As such, the examiner is able to define mixing level and residence time of fluid elements. A combined analysis of the Eulerian and the Lagrangian processing results of the LV-flow data provides a deeper insights into the complex flow scenario at hand.

In future, the definition of clear vortex boundaries using a local detection method should be studied, in order to provide easier observation of the time-dependent vortex behavior, i.e. vortex velocity. Additionally, different ways to adapt the FTLE method to heart flows will be examined including longer integration times, finer grids, detection of inflow and outflow regions in different integration times and calculations of residence times of particles in the heart. Finally, is desirable to evaluate the numerical experiments with measured flow data. Current efforts at ISTM include investigations to overcome the limited optical access of such flow scenarios based on 3D particle tracking. Future investigations foresee comparison of computational results with data obtained from optical measurements, i.e. volumetric velocimetry.

References

Blazevski, D., Haller, G. (2014). Hyperbolic and elliptic transport barriers in three-dimensional unsteady flows. *Physica D, 273-274*, pp. 46-64

Chong, M., Perry, A., & Cantwell, B. (1990). A general classification of three-dimensional flow fields. *Phys of Fluids A: Fluid Dynamics(1989-1993)*, pp. 765-777.

Gharib, M., Rambod, E., Kheradvar, A., Sahn, D. J., Dabiri, J. O. (2006). Optimal vortex formation as an index of cardiac health. *Proceedings of the National Academy of Sciences 103(16),* pp. 6305–6308

Grigoriev, R. O. (2012). Mixing in laminar fluid flows: From microfluidics to oceanic currents. *Transport and Mixing in Laminar Flows: From Microfluidics to Oceanic Currents*, pp. 1-4.

Haller, G., Yuan, G. (2000). Langrangian coherent structures and mixing in two-dimensional turbulence. *Physica D: Nonlinear Phenomena, 147(3)*, pp. 352-370.

Haller, G. (2002). Langrangian coherent structures from approximate velocity data. *Phys of Fluids, 14(6)*, pp. 1851-1861.

Haller, G. (2011). A variational theory of hyperbolic langrangian coherent structures. *Physica D: Nonlinear Phenomena, 240(7)*, pp. 574-598.

Hendabadi, S., Bermejo, J., Benito, Y., Yotti, R., Fernández-Avilés, F., Álamo, J. C., et al. (2013). Topology of Blood Transport in the Human Left Ventricle by Novel Processing of Doppler Echocardiography. *Annals of Biomedical Engineering, 41(12)*, pp. 2603-2616.

Hunt, J., Wray, A., Moin, P. (1988). Eddies, streams, and vonvergence zones in turbulent flows. In *Studying Turbulence Using Numerical Simulation Databases, 2,* pp. 193-208.

Jeong, J., Hussain, F. (1995). On the identification of a vortex. *Jounal of fluid mechanics*, pp. 69-94.

Kantz, H. (1994). A robust method to estimate the maximal lyapunov exponent for a time series. *Physics letters A, 185(1)*, pp. 77-87.

Pierrehumbert, R. (1991). Large-scale horizontal mixing in planetary atmospheres. *Phys of Fluids A: Fluid Dynamics (1989-1993), 3(5)*, pp. 1250-1260.

Shadden, S. C., Lekien, F., & Mardsen, J. E. (2005). Definition and properties of lagrangian coherent structures from finite-time Lyapunov exponents in two-dimensional aperiodic flows. *Physica D: Nonlinear Phenomena, 212(3)*, pp. 271-304.

Spiegel, K. (2009). Strömungsmechanischer Beitrag zur Planung von Herzoperationen. *Dissertation at Karlsruhe Institute of Technology.*